# Supporting information

## Great Chiral Fluorescence from Optical Duality Silver Nanostructures Enabled by 3D Laser Printing

Hongjing Wen,[ab] Shichao Song,[a] Fei Xie,[a] Bin Wang,[b] Jian Xu,[a] Ziwei Feng,[a] Shiyu Wu,[a] Jing Han,[a] Bai-ou Guan,[a] Xiaoxuan Xu,*[b] Yaoyu Cao,*[a] and Xiangping Li[a]

[a.] Guangdong Provincial Key Laboratory of Optical Fiber Sensing and Communications, Institute of Photonics Technology, Jinan University, Guangzhou 511443, P. R. China.
[b.] The Key Laboratory of Weak-Light Nonlinear Photonics, Ministry of Education, School of Physics, Nankai University, Tianjin 300071, China.

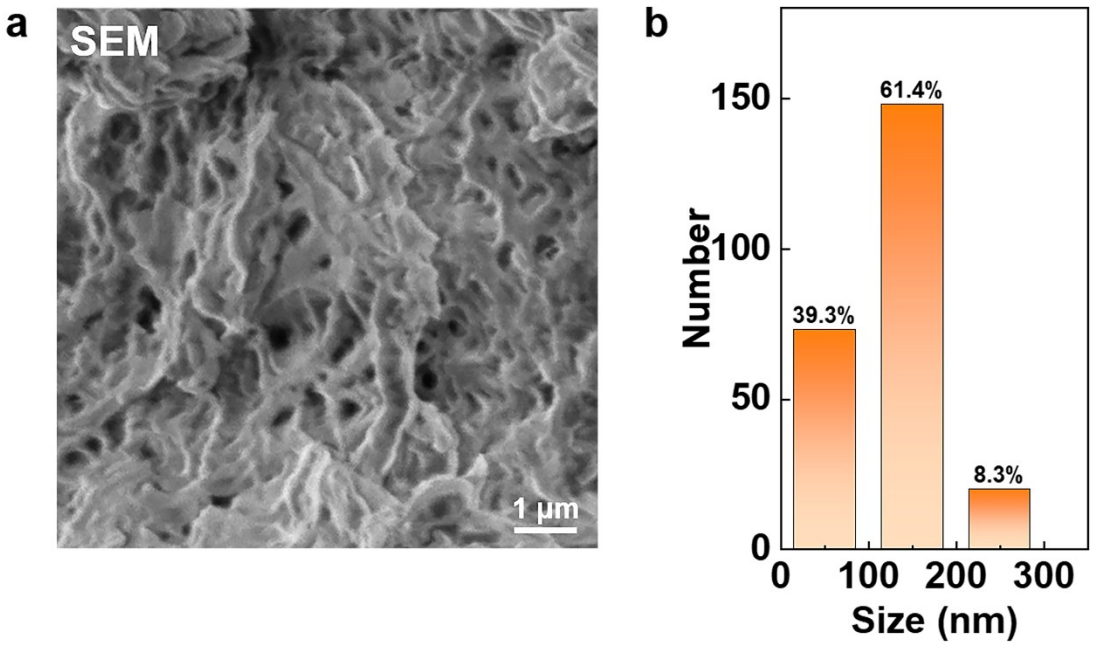


**Fig. S1. Characterization of agarose matrix. a** Scanning electron microscopy imaging of 7% weight-volume ratio agarose matrix. **b** The size statistical distribution of the pore structures in agarose.

The agarose for SEM measurement was prepared via freeze-drying method. According to the SEM image, the average size of the pores is less than ~150 nm. Therefore, the special pore structures in agarose make the agarose matrix an intercalating polymer network which could afford scaffoldings to support 3D consecutive metallic structures.

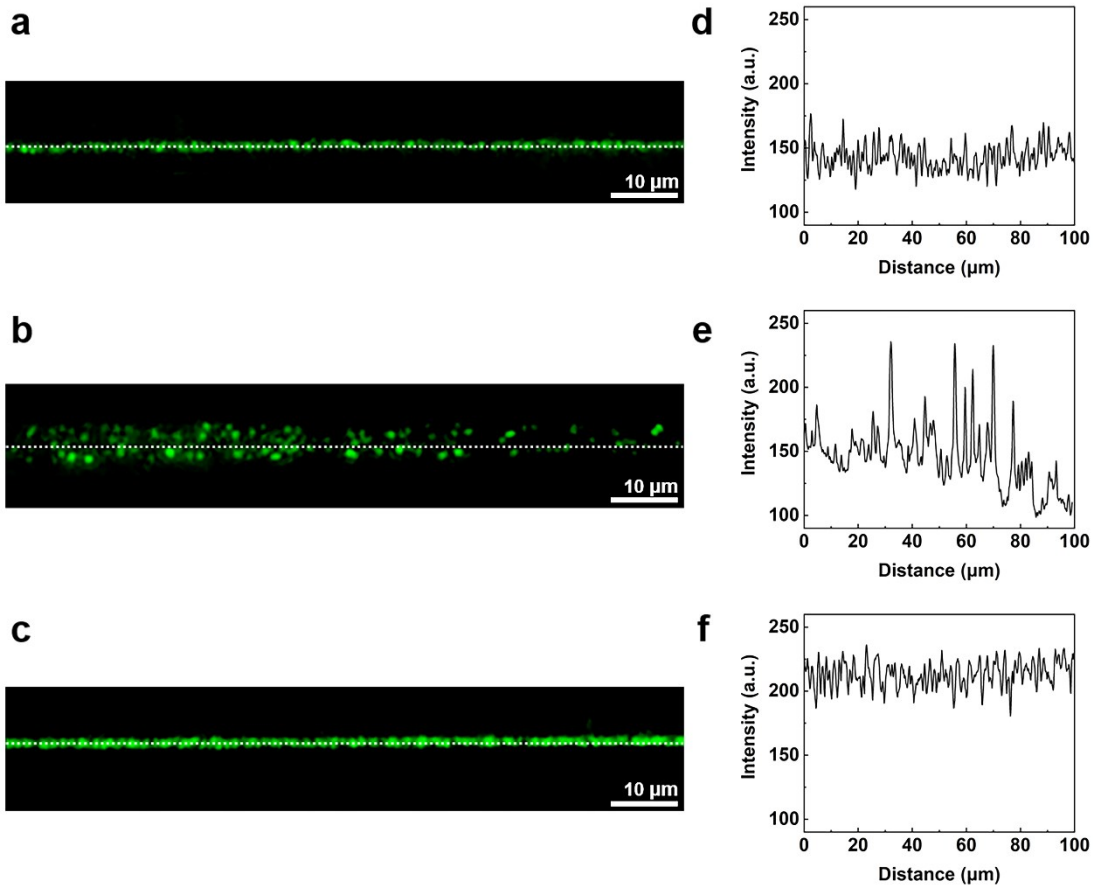


**Fig. S2. Silver wire structures produced via laser printing with different hydrogels.** The printing power is 1 mW and the printing speed is 10 μm/s. **a-c** The dark-field images of silver wire structures fabricated in polyethylene glycol diacrylate (PEGDA), sodium alginate, and agarose (5% w/v, weight-volume ratio), respectively. **d-f** The corresponding scattering intensity of the silver wires.

The silver wire structures were fabricated in different strains of hydrogels with the same printing laser power and scanning speed. Since the fluorescence and scattering uniformity of the photoluminescent structure are related to the porosity density in hydrogel, a suitable pore density will enhance the uniformity of the photoluminescent structure, which can offer a dense porosity scaffolding that provides a more uniform photoreduction position linked to the scaffolding. Here, it can be found from the scattering intensity distribution that the silver wire in agarose renders more reduced silver in favor of improving structural continuity for subsequent patterning compared to PEGDA and sodium alginate hydrogel host. These three common hydrogels with same concentration shows the agarose is the best candidate due to the denser porosities in agarose matrix. The other two hydrogel matrix can also support the exquisite photoluminescence uniformity with a certain concentration.

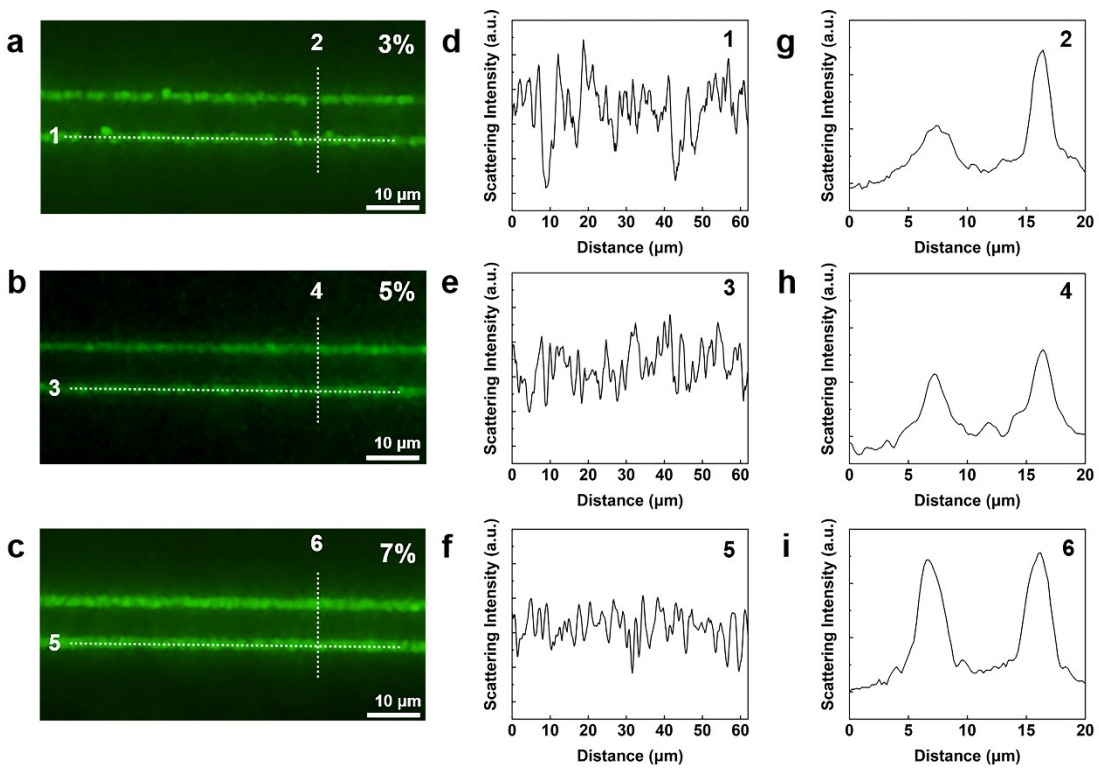


**Fig. S3. Silver wire structures printed in agarose of varied weights.** The printing power is 1 mW and the printing speed is 10 μm/s. (**a-c**) The dark-field images of silver wires structures processed in different weight-volume ratio (3%, 5%, 7% w/v) of agarose matrix. (**d and g**, **e and h**, **f and i**) The scattering intensity of the corresponding marked lines (Line 1 and 2 in **a**, Line 3 and 4 in **b**, Line 5 and 6 in **c**) on the silver lines structures. All the scale bar is 10 μm.

The density of agarose increases progressively as the weight-volume ratio of agarose matrix becomes greater from 3% to 5% w/v. And the higher agarose matrix density helps develop the uniform distribution of the silver nanoparticles. However, while the weight-volume ratio exceeds 7% w/v, the agarose matrix with increasing crosslinking density halts silver ammonia solution entering into the scaffoldings, leading to a decrease in the amount of photoreduced silver nanoparticles. Therefore, the agarose content is adopted at ~7% for scaffolding the silver structure as fabricated with reasonable structural continuity and stability.

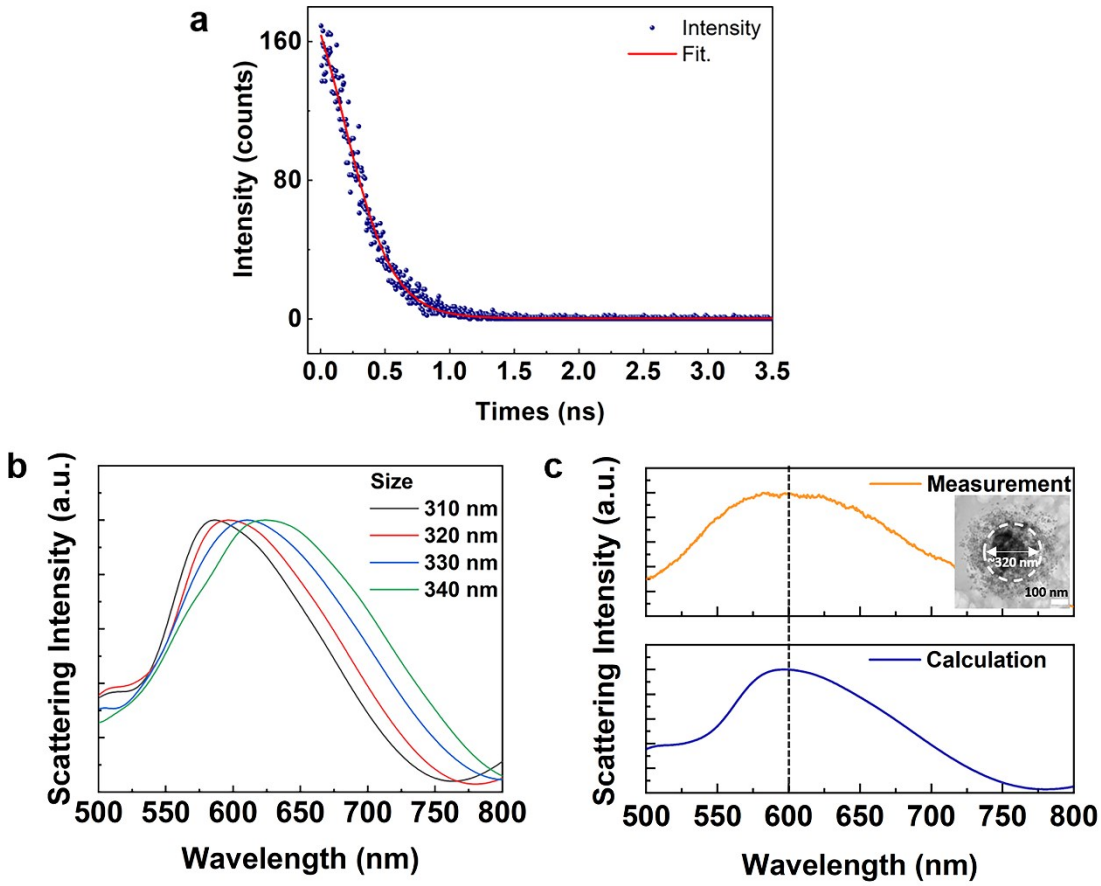


**Fig. S4. Optical properties of silver nanoclusters. a** The impulse response of the emission fluorescence for a silver nanocluster-based structure printed with the laser power of 1 mW at a printing speed of 10 μm/s. **b** The simulated scattering spectra of silver nanodots with different sizes ranging from 310 nm to 340 nm. **c** The experimental scattering spectra of a silver nanodot with the printing power of 1 mW and the exposure time of 80 ms. The corresponding simulated results of the scattering spectra of silver nanodots reveals an effective particle size of 320 nm. The inset shows the TEM of the corresponding silver nanodots.

The impulse response of the emission fluorescence which indicates the fluorescence lifetime of silver nanoclusters is less than 0.5 ns for a silver nanocluster-based structure printed with the laser power of 1 mW at a printing speed of 10 μm/s. The fitting curve presents the relationship between fluorescence intensity $y$ and time $t$ as the expression $y = 225.37906 \cdot \exp(-t/0.33654) - 0.18603$. With gradually increasing sizes of the silver nanodots varying from 310 nm to 340 nm, the relevant resonant wavelengths of the scattering spectrum redshift from 587 nm to 624 nm. The experimental scattering spectrum for the silver dot fabricated with the printing power of 1 mW and the exposure time of 80 ms is closed to the simulation spectrum with size of 320 nm. The broader scattering bandwidth in the experimental spectrum can be attributed to the fact that the morphology of the silver nanodots as fabricated prefers to be an ellipsoid rather than a perfect sphere.

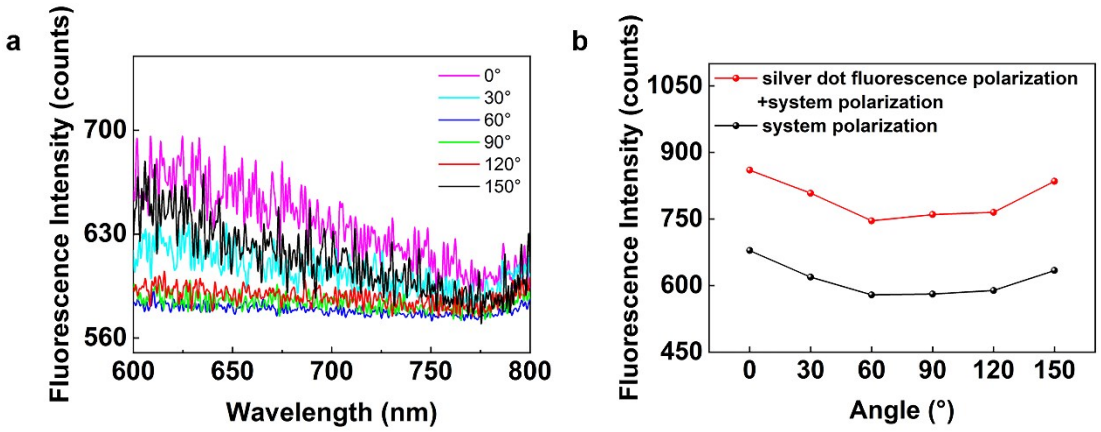


**Fig. S5. Polarization photoresponsivity of silver nanocluster/agarose matrix composite system. a** Fluorescence spectra of silver nanoclusters/agarose matrix composite system measured at different polarization angles from 0° to 150°. **b** The fluorescence intensity variances of rhodamine 6G and silver nanocluster/agarose matrix composite system at the wavelength of 630 nm indicating the intrinsic polarization performance of the detection system (black line) and the fluorescence polarization characteristic of silver nanocluster (red line).

A linear Polarizer (LP) is added into the emission collecting path to collect the fluorescence signal with different polarization angles. The non-polarized fluorescent material (rhodamine 6G) can determine the inherent polarization performance of the detection system. Rotating the linear polarizer, a series of spectra with respect to varied polarization angles can be obtained. And then, the fluorescence intensity at 630 nm is selected to manifest the relationship between the polarization angle and the fluorescence intensity, which reflects the polarization characteristic of the system (black line). Replacing the rhodamine 6G with a single silver nanodot, we obtain a sequence of spectra of the silver nanocluster fluorescence in the same way, and then take the intensity at 630 nm with different polarization angles (red line).

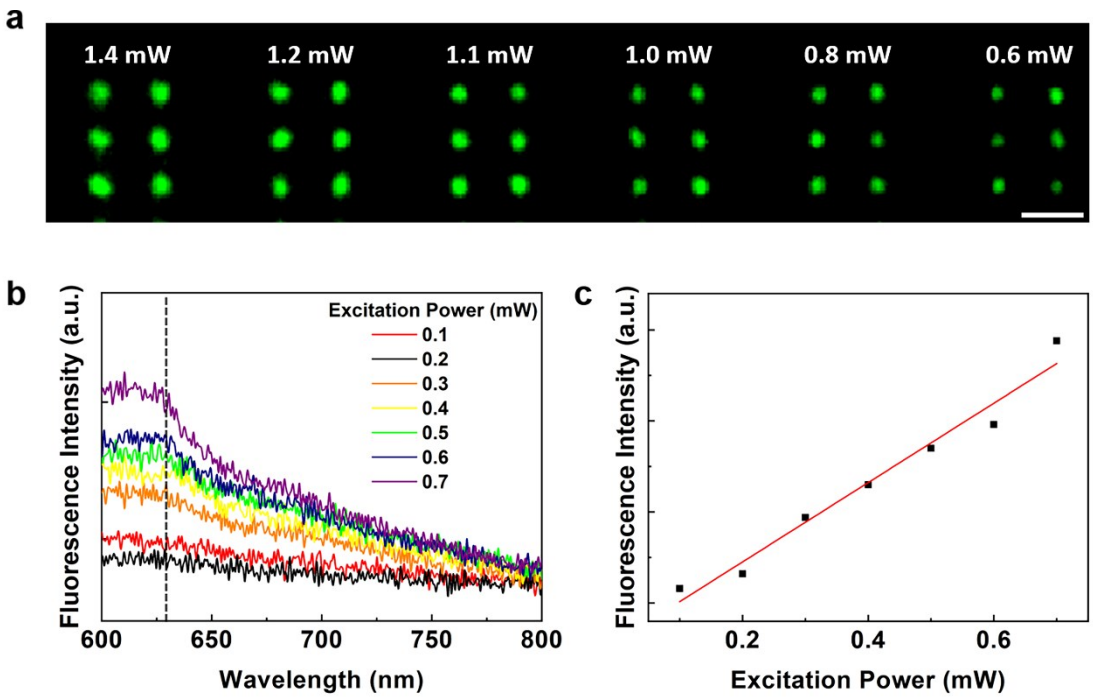


**Fig. S6. Fluorescent characteristic of silver dots arrays with different printing and excitation powers. a** A dark-field scattering image of silver dots matrixes (2×3) fabricated with different printing power (1.4 mW, 1.2 mW, 1.1 mW, 1.0 mW, 0.8 mW, 0.6 mW) at the fixed exposure time of 80 ms. The scale bar is 5 μm. **b** Fluorescence emission spectra of a silver nanodot structure in agarose matrix obtained with CW laser excitation ($\lambda_{exc}$ = 532 nm). The excitation power ranges from 0.1 mW to 0.7 mW. **c** The fluorescence intensity of silver dot structure depending on the excitation power measured at 630 nm.

Greater laser printing power enlarges the printing region for a single laser focal spot with the laser intensity above the fabrication threshold for the generation of silver dot, which makes the size of silver dot directly proportional to the printing power. Besides, we explored the impacts of the excitation power (0.1-0.7 mW) on the fluorescence intensity of silver nanodot structure with 0.2 mW-printing power and 80 ms-exposure time. The fluorescence intensity at the wavelength of 630 nm varies linearly with the excitation power, showing obvious single photon characteristics.

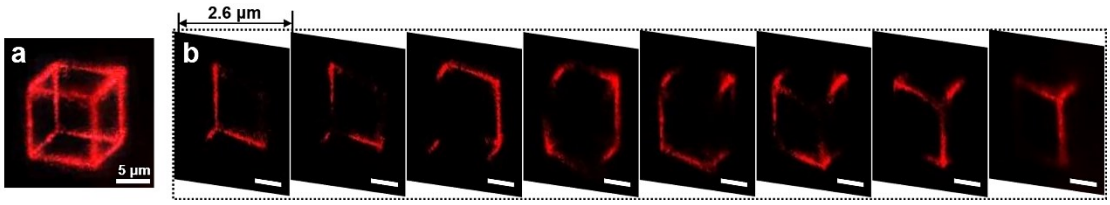


**Fig. S7. Fluorescence images of a silver cubic nanostructure.** The silver cubic nanostructure is fabricated with the laser power of 1 mW and printing speed of 5 μm/s captured by confocal microscope. **a** Digital composite of multiple layer images from a cube silver nanostructure. **b** The microscope confocal images of the cube structure obtained by layer-by-layer scanning (~2.6 μm layer distance). All the scale bars are 5 μm.

The images were acquisitioned by multiple layer scanning with a confocal microscope where a 100× oil objective (NA = 1.4) is adopted. The 3D confocal image of the cube structure can be achieved with layer-by-layer scanning with a 532 nm CW laser excitation. The excitation power is fixed at 200 μW. Eventually, the whole 3D confocal fluorescent image can be digitally matched up with hierarchical scanning images. While a bit fluctuation of confocal fluorescence intensity in the perspective view (**a**) comes from the image mosaic errors and the scanning layer distance during the multilayer scanning (**b**).

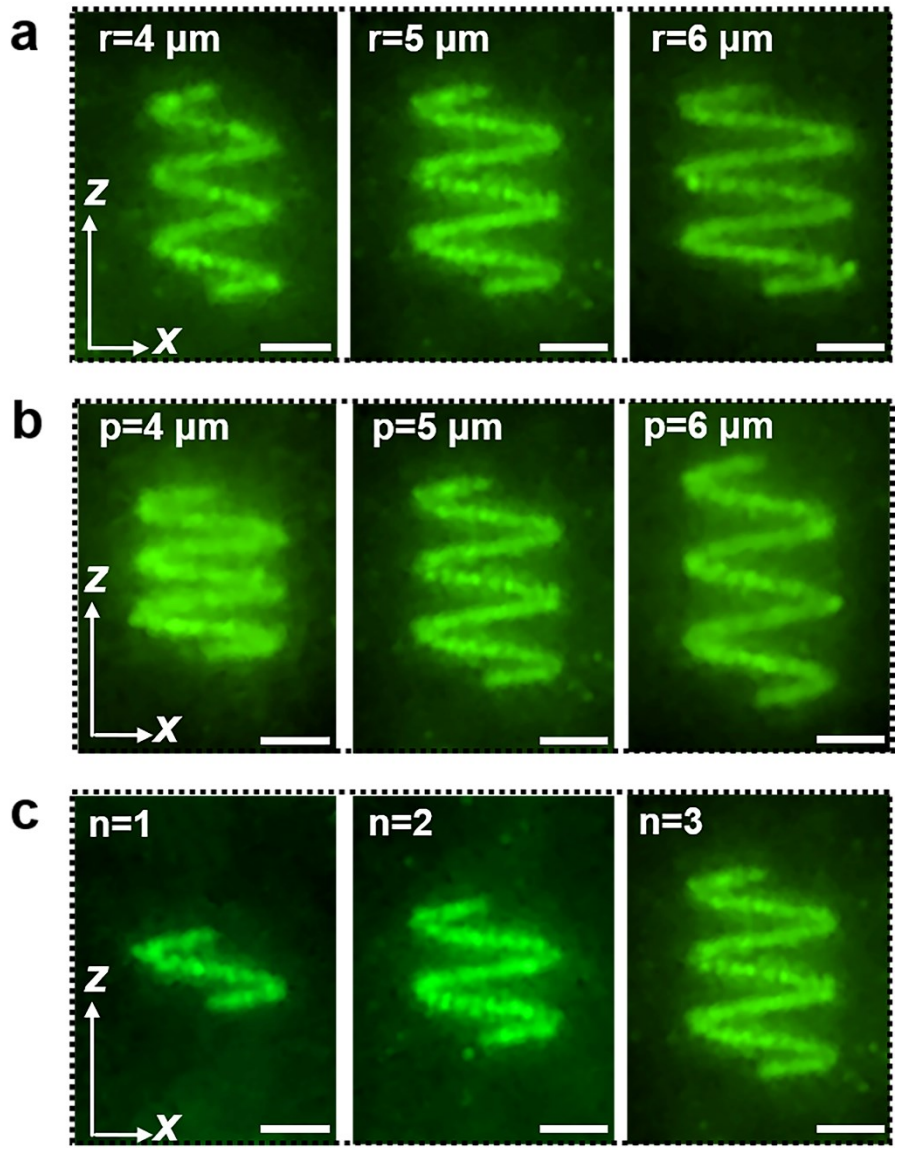


**Fig. S8. Dark field images of silver spiral structures with different characteristic parameters (radius (*r*), pitch (*p*) and the number of turns (*n*)).** The printing laser power is 1 mW and the scanning speed is 30 μm/s. **a** The scattering images of silver spiral structures with $p$ = 5 μm, $n$ = 3 and radii $r$ of 4, 5, 6 μm on the side view. **b** The side-view scattering images of silver spiral structures with $r$ = 5 μm, $n$ = 3 and pitches $p$ of 4, 5, 6 μm. **c** The side-view scattering images of silver clusters spiral structures with $r$ = 5 μm, $p$ = 5 μm and the number of turns $n$ of 1, 2, 3. All scale bar are 5 μm.

We can achieve arbitrary helical structures with different radii ($r$), pitches ($p$) and number of turns ($n$) via laser printing. Moreover, the scattering images of these 3D helical structure show excellent morphological shapes, which may shed light on versatile 3D or 4D silver functionalized devices.

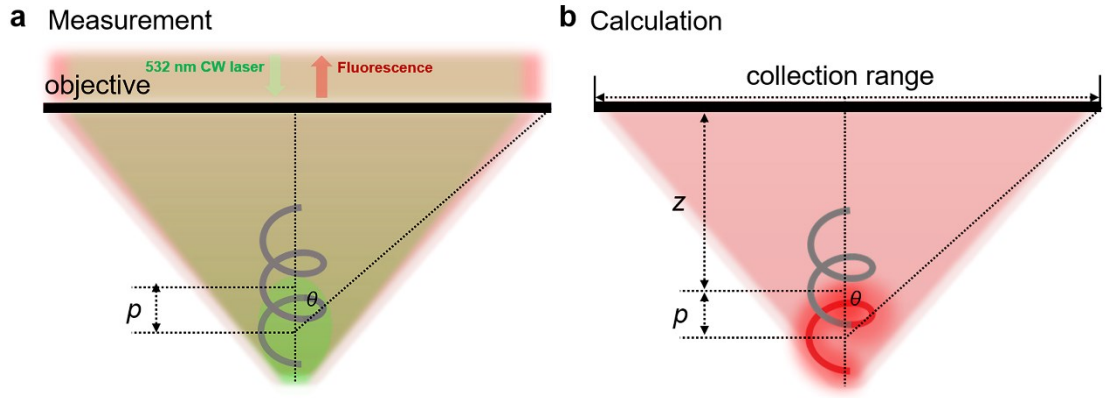


**Fig. S9. Schematics of measured collection system and simulation model. a** The schematic of experimental measurement. **b** The setting schematic of FDTD simulation model. In simulation or calculation, the helix radius, linewidth and pitch in simulations are bounded to the corresponding experimental measurements.

Taking the shape of the excitation laser focal spot (532 nm CW laser) into account (~780 nm-focal length), the photoluminescence only occurs at parts of helical structure in the tightly focused light field. In order to ensure the accuracy of simulation, the simulation models are set in reference to the experimental setups. Hence, a plurality of dipoles arranged at the surface of helical structure in the tightly focused light filed are used as the fluorescence source. Meanwhile, the span of power profile monitor in simulation depends on the NA of the measured objective lens, The collection angle in measure can be calculated as follows: $\theta = \arcsin(NA/background\ index)$, therefore, the span of monitor could be set as $2\tan\theta \times z$, where $z$ is the distance between monitor and focal spot in z-direction. In order to achieve the greatest light-matter interaction, the 532 nm CW laser is focused to the bottom of the helical structure (which is the far end of the helix to the detector). And then, the bottom circle of the helix structure is excited to generate a fluorescent signal to be detected by the spectrometer.

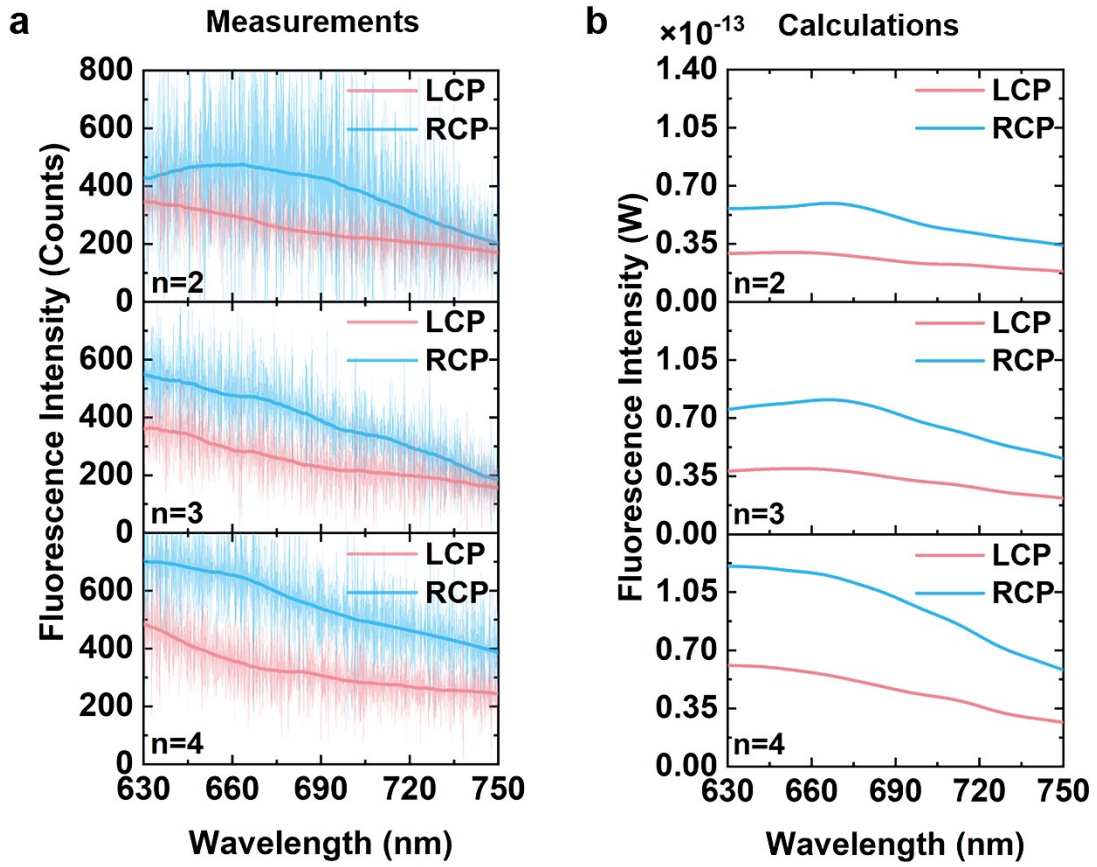


**Fig. S10. LCP and RCP fluorescence spectra of silver nanocluster-based helix nanostructures.** The fluorescence spectra are obtained through (**a**) measurements with the turns of 2, 3, 4 from top to bottom and (**b**) the corresponding FDTD calculations, respectively.

For a clockwise spiral structure, the fluorescent intensity of right-handed polarized light passing through the structure is greater than that of left-handed polarized light due to the light-matter interaction between the light with left-handed circular polarization and left-handed structure (J. K. Gansel, et al. *Science* 325, 1513 (2019)). It can be seen from the simulation result that the spectral intensity at the short wavelength is higher than that at the long wavelength, which is because the intensity of the silver nanocluster fluorescence spectra at the short wavelength are significantly higher than that at the long wavelength, and they are consistent with the trend of the inherent fluorescence spectra of silver nanoclusters. The theoretically calculated spectra with right-handed and left-handed circular polarization are both normalized. However, in experiment, the total number of emitted fluorescent photons is difficult to count accurately, and thus, the absolute photon counts of transmitted fluorescence with right-handed and left-handed circular polarization are used to indicate circular dichroism (The difference, i.e., CD can be seen in Fig. 4, Main text). The variation tendencies of experimental fluorescence spectra are in good agreement with the ones obtained by simulations.